Journal of the Physical Society of Japan **88**, 124705 (2019)
https://doi.org/10.7566/JPSJ.88.124705

Giant Rashba-Type Spin Splitting in Bi/Ag(111) from Asymmetric Interatomic-Hopping

Jisook Hong[1], Jun-Won Rhim[2,3,4], Inkyung Song[3], Changyoung Kim[3,4], Seung Ryong Park[5]*, and Ji Hoon Shim[1,6]†

[1]*Department of Chemistry, Pohang University of Science and Technology, Pohang 37673, Korea*
[2]*Max-Planck-Institut für Physik komplexer Systeme, 01187 Dresden, Germany*
[3]*Center for Correlated Electron Systems, Institute for Basic Science, Seoul 08826, Korea*
[4]*Department of Physics and Astronomy, Seoul National University, Seoul 08826, Korea*
[5]*Department of Physics, Incheon National University, Incheon 22012, Korea*
[6]*Department of Physics and Division of Advanced Nuclear Engineering, Pohang University of Science and Technology, Pohang 37673, Korea*

(Received July 23, 2019; accepted October 7, 2019; published online November 11, 2019)

Rashba-type spin splitting (RSS) has recently drawn added attention due to its central role in the field of spintronics. In that regards, designing materials with giant RSS is highly desirable for practical spintronic applications, and thus disclosing the origin of the giant RSS could pave the way. Here, we theoretically demonstrate that the giant RSS observed in Bi/Ag(111) alloy system emerges from the difference in kinetic energy or interatomic-hopping strength, not from a uniform electric field. Our density functional theory calculation and tight-binding analysis show that depending on the chirality of orbital angular momentum (OAM), the Bi orbital forms an asymmetric charge distribution in the direction towards or away from the Ag atom. As a result, opposite OAM chirality results in difference in hopping strength between Bi and Ag orbitals, and this kinetic energy difference dominates the size of RSS. This new interpretation on the RSS successfully explains the giant RSS in Bi/Ag(111) surface states and has implication for the RSS mechanism in general.

1. Introduction

There has been a recent surge in the study of Rashba-type spin splitting (RSS) due to its role in the field of spintronics[1–3] as exemplified by spin field effect transistor,[4,5] spin orbit torque,[6,7] and spin to charge conversion studies.[8–10] In addition to achieving controllability of the splitting,[11–13] an important direction in the research is to increase the splitting energy. For that reason, there have been extensive studies on the so-called giant RSS systems such as Bi/Ag(111), Pb/Ag(111),[14–19] and BiTeI.[20–23] However, the exact mechanism for the giant RSS has been relatively poorly understood.

RSS was conventionally thought to be from an effective Zeeman coupling between the electron spin and a relativistic magnetic field for a moving electron in an electric field,[24] but it was recognized that its energy scale is too small to induce the split energy.[25,26] It was recently shown that local orbital angular momentum (OAM) induces an electric polarization, and its coupling to the electric field can fully account for the scale of the energy splitting in typical systems with strong spin–orbit coupling (SOC) such as Bi(111) surface states.[27–29] Please note that the local OAM means the OAM near nuclei in a solid.[27–30] This description, however, has been challenged by extraordinarily giant RSS found in several materials.[14,20] Recently, the role of hopping energy, which is mostly kinetic energy, for giant RSS has been highlighted in $PtCoO_2$ and $PdRhO_2$ although the RSS sizes in these cases are determined by atomic SOC rather than the hopping energy.[30] It has been also reported that formation of hybridization states between Ag and Bi by electron hopping plays a crucial role for the RSS in Bi/Ag(111) alloy system.[31] Uncovering the mystery of the giant RSS is important not only in the fundamental scientific point of view but also for possible device applications.

In this work, we pay our attention to a possibility that hopping energy can effectively work as the inversion symmetry breaking (ISB) field in Bi/Ag(111) alloy system and, in turn, determines the size of RSS as well. More specifically, we focus on asymmetric charge distribution due to the local OAM and its role in hopping energy. Our density functional theory (DFT) calculation and tight binding (TB) analysis show that the different charge configurations result in asymmetric interatomic-hopping. The energetics of the giant RSS is determined by the difference in hopping energy between the spin split bands, which is clearly contradictory to the theories proposed earlier. The RSS of Bi/Ag(111) alloy should be the first system for which RSS size is found to be determined by the kinetic energy rather than potential-type energies such as effective Zeeman splitting, electrostatic energy and SOC. Our new picture should be applicable to other systems with large RSS.

2. Methods

2.1 *DFT calculation*

For non-collinear DFT calculations, we use Vienna Ab initio Simulation Package (VASP)[32–35] and OpenMX codes.[36–38] Using VASP code with the generalized gradient approximation of Perdew–Berke–Ernzerhof (GGA-PBE),[39] we optimize the lattice constant of *fcc* Ag until the internal atomic force becomes less than 10^{-8} eV/Å using $15 \times 15 \times 15$ mesh to sample k-points without considering SOC to get $a = 4.15$ Å. From the lattice constant, we construct the structures of Bi/Ag(111) and $BiAg_2$, and calculate the band structures and spin/OAM textures of $BiAg_2$ using $7 \times 7 \times 1$ k-mesh taking account of SOC to observe Rashba-type spin splitting. By taking Ag away from $BiAg_2$, we construct Bi triangular monolayer and calculate the electronic structures. For analysis on the orbital composition of the Rashba-split bands, we use OpenMX code with $s2p2d2$ pseudo-atomic basis orbitals and PBE potentials for Bi and Ag atoms.

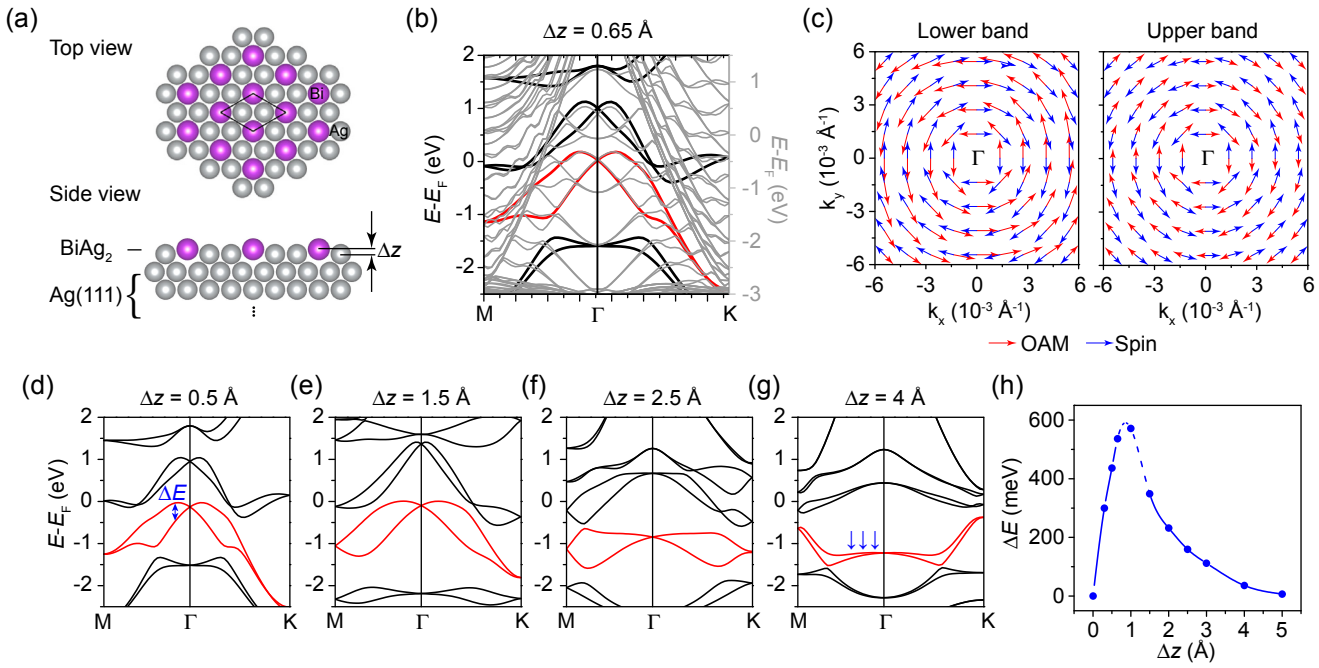

Fig. 1. (Color online) Crystal and electronic structures of Bi/Ag(111) and $BiAg_2$. (a) Crystal structures of Bi/Ag(111) and its topmost layer $BiAg_2$. Crystal structures are illustrated by using VESTA.[42] (b) Electronic structures of $BiAg_2$ (left axis, black and red thick lines) and Bi/Ag(111) (right axis, grey thin lines) at $\Delta z = 0.65$ Å. (c) Spin and OAM textures of $J \approx 1/2$ bands of $BiAg_2$ in reciprocal **k**-space. (d–g) Electronic structures of $BiAg_2$ for various Δz values. Red lines denote the Bi $J \approx 1/2$ bands. The position of k_1 (right), k_2 (middle), and k_3 (left) is marked in (g) with blue arrows. (h) The size of RSS at $k = 0.02$ Å^{-1} (ΔE) as a function of Δz. The maximum ΔE value occurs when Δz is in between 0.65 and 1.5 Å.

2.2 *Tight binding approach*

For the analytic analysis of relations between the RSS, $\Delta\langle H_{sp}\rangle$, and $\Delta\mathrm{Ag}(s)$, we investigate the minimal TB model, and analyze it within the perturbation theory. Based on DFT calculations, we construct a minimal TB model with only *s*- and *p*-orbitals. We consider, for each spin, one *s*-orbital at each of two Ag atoms in the unit cell, and p_x-, p_y-, and p_z-orbitals at Bi atom. In total, we have ten orbitals in a unit cell. Hamiltonian matrix elements are obtained following the Slater–Koster's scheme.[40] We find four parameter sets for the bond integrals that qualitatively reproduce the giant RSS and overall band structure at $\Delta z = 0.65$, 3, 4, and 5 Å. More details on TB analysis are described in the Supplementary Information.[41]

3. Results

In Fig. 1(a), we present the crystal structure of Bi/Ag(111) alloy system. It was previously noticed that the surface states are strongly localized in the topmost $BiAg_2$ layer.[43] We confirm this from the fact that the band structures of Bi/Ag(111) and $BiAg_2$ monolayer show almost identical giant RSS [Fig. 1(b)]. Figure 1(c) shows the chiral spin and OAM textures of the split bands of $BiAg_2$, which clearly reproduce the essential features of Bi/Ag(111) surface states.[44] As the Rashba states are almost the same, we continue our discussion based on the $BiAg_2$ for the sake of simplicity (no bulk states present). $BiAg_2$ monolayer is composed of Bi triangular lattice and neighboring Ag hexagonal lattice as shown in the top view in Fig. 1(a).

It has been known that the size of RSS in $BiAg_2$ is highly sensitive to the buckling distance Δz between Bi and Ag layer.[15,43] In Figs. 1(d)–1(g), we present the band structures for various Δz values and highlight the Bi $J \approx 1/2$ bands (red lines) which show the largest RSS. The splitting energy (ΔE) against Δz is depicted in Fig. 1(h). As expected, there is no splitting when Δz is zero since there is no ISB. As Δz increases, ΔE initially increases very sharply. It hits the maximum at $\approx$1 Å and then decreases. When Δz is far enough, the band structure becomes independent bands of Ag hexagonal lattice and Bi triangular monolayer. In the most stable configuration, it is known that Δz is around 0.65 Å.[45] The electronic structures of Bi/Ag(111) and $BiAg_2$ for $\Delta z = 0.65$ Å are shown in Fig. 1(b).

We first check out the possibility that the giant RSS is induced by a uniform surface field. Since the Rashba-split bands of $BiAg_2$ are mostly Bi bands, we consider Bi triangular monolayer under an external perpendicular field as an simplified model for $BiAg_2$ [Fig. 2(a)]. In order to study the possible surface field, we compare the ΔE of $BiAg_2$ and Bi triangular monolayer under an external field. We plot the band structure of Bi monolayer under $E_{\mathrm{ext}} = 0.5$ V/Å in Fig. 2(b). The overall band structure of Bi monolayer is comparable to that of $BiAg_2$ when $\Delta z = 4$ Å. The pair of bands colored in red is mainly from Bi $J \approx 1/2$ states and shows a RSS energy of 29 meV at $k = 0.06$ Å^{-1}, which is much smaller than the value observed in $BiAg_2$. In $BiAg_2$, Bi $J \approx 1/2$ states which is mostly coming from Bi p_z-orbital show the largest RSS, whereas Bi $J \approx 2/3$ states crossing the Fermi level show the largest RSS in Bi monolayer case. In Fig. 2(c), we plot ΔE of Bi triangular monolayer as a function of the applied field strength E_{ext}. The ΔE increases linearly with E_{ext} as the linear fit shows (red line). Based on the extrapolation of the data, one can estimate the E_{ext} required to split the $J \approx 1/2$ bands of Bi as much as those of $BiAg_2$. A few cases for different values of Δz are presented with blue empty circles in the figure. One can see that a field

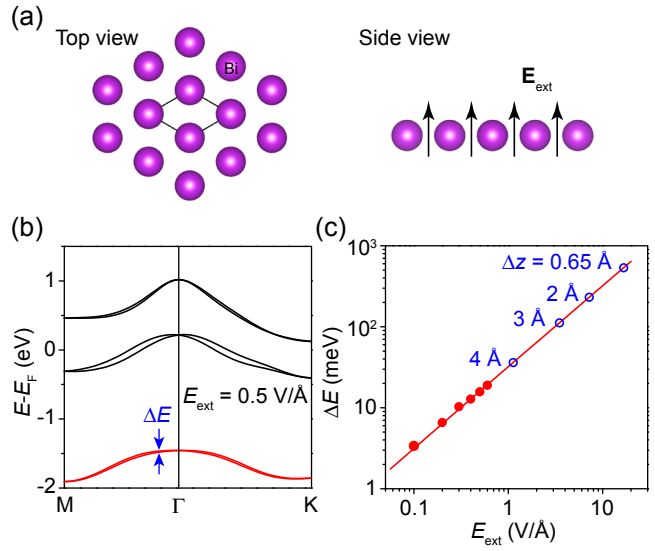

Fig. 2. (Color online) Crystal and electronic structures of Bi monolayer under an external electric field. (a) Crystal structure of Bi triangular monolayer. An external electric field E_{ext} is applied perpendicular to the Bi plane. (b) Electronic structure of Bi monolayer under $E_{\text{ext}} = 0.5\,\text{V/Å}$. $J \approx 1/2$ bands are shown in red. (c) The splitting energy at $k = 0.02\,\text{Å}^{-1}$ (ΔE) as a function of E_{ext}. Blue dashed lines represent the required E_{ext} for Bi monolayer to have the same ΔE of the $BiAg_2$ $J \approx 1/2$ bands, estimated at different Δz values.

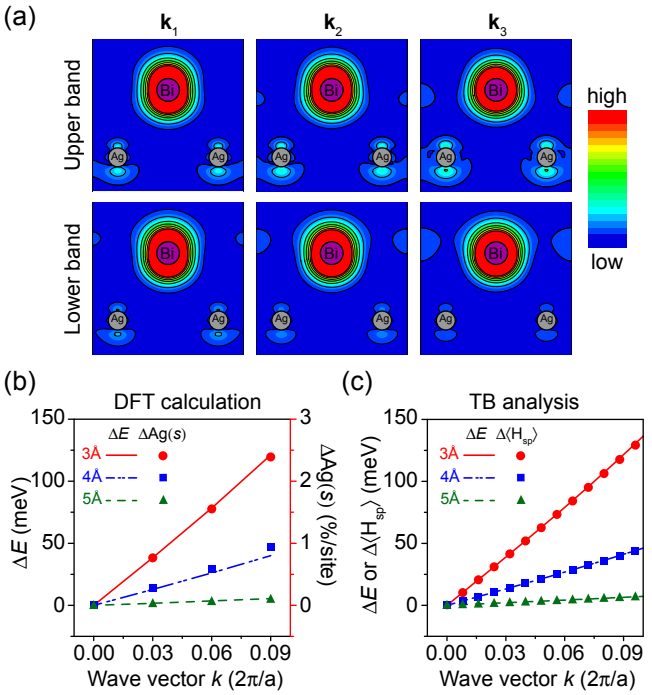

Fig. 3. (Color online) Partial charge densities and splitting energy. (a) Partial charge densities of the Rashba-split bands of $BiAg_2$ with $\Delta z = 4$ Å at selected $\mathbf{k}$-points of $\mathbf{k}_1 = (0.06, 0, 0)$, $\mathbf{k}_2 = (0.12, 0, 0)$, and $\mathbf{k}_3 = (0.18, 0, 0)$ in unit of $2\pi/a$. We merge partial densities of six symmetrically indistinguishable $\mathbf{k}$-points. (b) The size of splitting (left axis, lines) at wave vector $(k, 0, 0)$ and difference in Ag s-orbital contributions between the split bands (right axis, markers) from DFT calculations. (c) The size of splitting (lines) and the difference in the averages of s–p hopping energy between two split bands (markers) from TB calculations. More details on TB analysis are described in the Supplementary Information.[41]

stronger than $\sim 18\,\text{V/Å}$ is needed to make ΔE of Bi monolayer comparable to that of $BiAg_2$ with $\Delta z = 1$ Å. The TB analysis we considered in our previous study[29] also shows that we need to apply $E_{\text{ext}} \sim V_{sp\sigma}/V_{ppz}$ (eV/Å) $\sim$ 10 (eV/Å) to achieve a similar ΔE ($V_{sp\sigma}$ is the bond integral between s- and p-orbitals σ bond in $BiAg_2$, and V_{ppz} is the electric-field-induced hopping between neighboring p_z orbitals in the Bi monolayer). Considering typical values of work function (a few eV) and the length scale of the surface depth (a few Å),[26] it is unrealistic for Bi to have an effective field as strong as $\sim 18\,\text{V/Å}$ from Ag sublayer. This implies that the effective surface field is not the probable cause of the giant RSS observed in Bi/Ag(111).

In order to find the true mechanism of the giant RSS in $BiAg_2$, we perform DFT and TB analysis to investigate the interaction between Bi and Ag. In Fig. 3(a), we plot the partial charge densities of the Rashba-split bands projected on the (110) plane passing through Ag–Bi–Ag atoms. We note that when Bi and Ag are close, they form strongly hybridized states which are very complicated, making the analysis and intuitive understanding very difficult (see Fig. S5 and relevant text in Supplementary Information[41]). In Fig. 3(a), in order to demonstrate the mechanism in a more intuitive way without loosing the essential physics of RSS, we choose $z = 4$ Å, which allows us to distinguish the charge from Bi and Ag clearly and make the analysis easier. In addition to the obvious Bi p-orbital feature, there is contribution from Ag orbitals which indicates hybridization between Bi and Ag. Interestingly, there is a clear difference between the Ag contributions from the two Rashba-split bands; the partial charge density of the upper band has significant Ag contribution while the lower band has very little. As the momentum k increases away from the Γ-point, the difference becomes more distinct. The difference is accompanied by an asymmetric charge distribution around Bi. We can see in Fig. 3(a) that the Bi states in the upper band spreads downward while they move upward in the lower band. This behavior is reminiscent of the k-dependent asymmetric charge distribution induced by the existence of local OAM.[27–29] Here, we would emphasize that size of the local OAM was theoretically investigated as a function of Δz and was found to be still significant until down to $\Delta z = 0.65$ Å (for detail, see Supplementary Information[41]).

Based on the linear combination of pseudo-atomic orbitals (LCPAO) coefficients of the Rashba-split bands from DFT calculation, we quantitatively investigate the composition of the bands. In Fig. 3(b), we present ΔE and the difference in Ag s-orbital contributions [$\Delta\text{Ag}(s)$] which represents the hybridization strength between Bi and Ag for $\Delta z = 3$, 4, and 5 Å. Both ΔE and $\Delta\text{Ag}(s)$ increase linearly with k, and increase as Δz decreases. These results imply that OAM-induced asymmetric charge distribution around Bi results in different hybridization strength between Bi p- and Ag s-orbitals for the two split bands and that the difference in the hybridization dominates the energetics of RSS. At a smaller distance below $\Delta z = 2$ Å, however, it becomes difficult to use LCPAO analysis because all spd orbitals show complicated contributions in the covalent bonding between Bi and Ag atoms. We note that the two pairs of Bi $J \approx 3/2$ bands located above the Bi $J \approx 1/2$ bands have smaller RSS because the charge distributions of Bi $J \approx 3/2$ states has dumbbell-like shape, and is thus relatively less dispersive

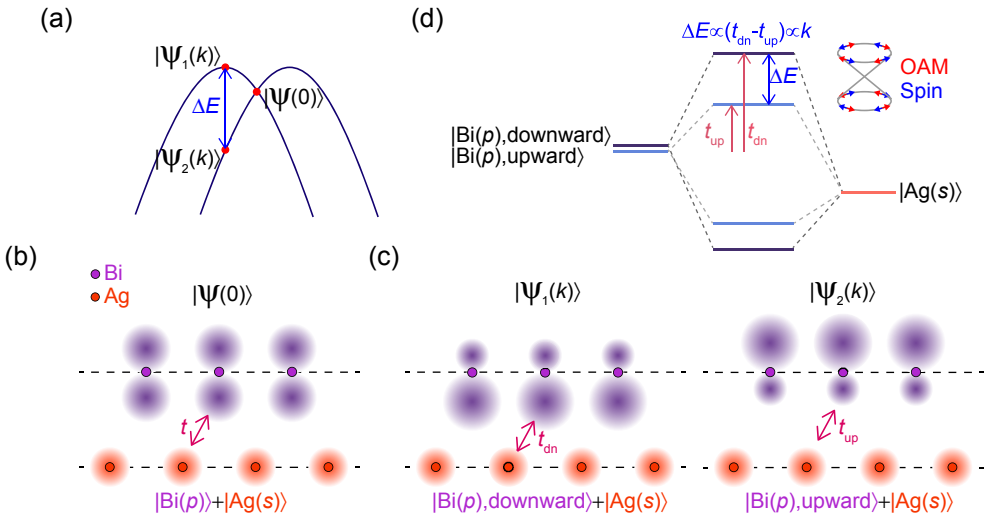

Fig. 4. (Color online) Schematic description of giant RSS mechanism. (a) Schematic band structure and wave functions. (b, c) Partial charge distributions at $k = 0$ and $k \neq 0$. (d) Orbital energy-level diagram for $BiAg_2$ and chiral spin/OAM of split bands.

along the z-direction.[29] This results in a smaller overlap or hybridization between Bi and Ag orbitals.

To examine the correlation between ΔE and anisotropic hybridization strength in Rashba-split bands analytically, we consider a TB model for $BiAg_2$ monolayer. From TB analysis (for detail, see Supplementary Information[41]), we derive a Rashba Hamiltonian of the form

$$H_R = E_\Gamma \sigma_0 + \alpha_R \mathbf{k} \times \boldsymbol{\sigma} \cdot \hat{z} \tag{1}$$

around the Γ-point where $\alpha_R = 4\sqrt{3} V_{sp\sigma} A_s A_{xy}$ and σ_i is the Pauli matrix. Here, A_s and A_{xy} are amplitudes of s- and $p_{x(y)}$-orbitals at the Γ-point. We assume that the lattice constant is equal to 1 for convenience. This leads to $\Delta E \approx 8\sqrt{3}|V_{sp\sigma}|A_s A_{xy} k$ and is well described by $\Delta\langle H_{sp}\rangle$, the difference between the averages of s–p hopping energy between the two Rashba-split bands as shown in Fig. 3(c). Equation (1) implies that the giant RSS stems from the large value of $V_{sp\sigma}$ (≈ 1 eV) and the high s- and $p_{x(y)}$-orbital contents. ISB makes A_s finite through the finite overlap between s- and p_z-orbitals, which allows the RSS. Then, the RSS is largely amplified by a large $V_{sp\sigma}$. These processes are simply characterized by $\Delta\langle H_{sp}\rangle$ in the long wavelength limit. We further show that $\Delta\langle H_{sp}\rangle$ is manifested as the physical quantity $\Delta\mathrm{Ag}(s)$ by the explicit formula

$$\Delta E \approx \gamma \Delta \mathrm{Ag}(s), \tag{2}$$

where γ is a constant evaluated from the eigenvalues and wave functions at the Γ-point.

Based on the DFT and TB analysis, we propose a mechanism of the asymmetric interatomic-hopping for RSS as schematically described in Fig. 4. Since $k = 0$ at the Γ-point, Bi p-orbital forms *symmetric* charge distribution centered at the Bi atom [Fig. 4(b)]. Thus, two spin bands are degenerate, as also required by the Kramers' theorem. Away from the Γ-point, asymmetric charge distribution around Bi develops as shown in Fig. 4(c) because of the local OAM in the $J \approx 1/2$ state and finite crystal momentum k.[27–29] We denote those states by $|\mathrm{Bi}(p), \mathrm{downward}\rangle$ and $|\mathrm{Bi}(p), \mathrm{upward}\rangle$, depending on how the wave function extends. Note that charge densities of the two states extend in opposite directions because the OAM chiralities are opposite for the two states as seen in Fig. 1(c). As a result, the two states have different hopping strength with Ag; $|\mathrm{Bi}(p), \mathrm{downward}\rangle$ and $|\mathrm{Ag}(s)\rangle$ have a considerable overlap and a large hopping parameter t_{dn}, while $|\mathrm{Bi}(p), \mathrm{upward}\rangle$ and $|\mathrm{Ag}(s)\rangle$ overlap less and thus have a smaller hopping parameter t_{up}. Consequently, the bonding and anti-bonding states of $|\mathrm{Bi}(p), \mathrm{downward}\rangle$ and $|\mathrm{Ag}(s)\rangle$ have larger energy shifts than those of $|\mathrm{Bi}(p), \mathrm{upward}\rangle$ and $|\mathrm{Ag}(s)\rangle$ as shown in Fig. 4(d). Because Bi p-orbital is higher than Ag s-orbital energetically, the anti-bonding states are mainly composed of Bi p-orbitals in terms of LCPAO. There are also Ag-dominant bonding states located at lower energy. In this discussion, we have focused on Bi p-orbital dominant anti-bonding states which show the giant RSS. Then, the energy difference between the two anti-bonding states determines the size of RSS. Note that the split energy is linear in k because the charge asymmetry is proportional to $\mathbf{k} \times \mathbf{L}$.

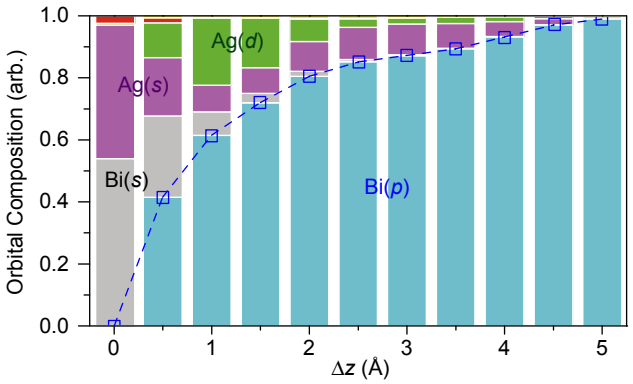

Fig. 5. (Color online) Δz dependent orbital composition at the Γ-point. Grey, blue, red, purple, and green color represent contributions from Bi s-, p-, d-, Ag s-, and d-orbitals, respectively. Dashed blue line is guide for eye.

In order to further discuss the change in the Δz dependent RSS, we plot in Fig. 5 the atomic orbital contributions of one Bi and two Ag atoms (or LCPAO coefficients) to the Rashba split bands at Γ-point against Δz. When Bi and Ag are separated more than 5 Å ($\Delta z \to \infty$), the bands are mostly composed of Bi p-orbitals and there is no Ag orbital

contribution. As Δz decreases, Bi and Ag orbitals start to hybridize and the RSS becomes larger until Δz is about 1 Å. When $\Delta z = 0$, the spin states mostly come from Bi and Ag s-orbitals which have no local OAM ($\mathbf{L} = 0$). As Δz decreases, the OAM decreases as well (see Fig. S6 in Supplementary Information[41]), which leads to less asymmetric charge distribution around Bi and thus vanishing spin splitting. Therefore, RSS in $BiAg_2$ takes the maximum value when $\Delta z \sim 1$ Å which gives the most asymmetric hopping strength between Bi and Ag.

4. Discussion

Our asymmetric interatomic-hopping induced RSS model tells us that the direction of spin/OAM chiralities can be controlled by relative energy levels of the surface and substrate atoms. In the case of Bi/Ag(111), the energy level of the Bi p-orbital lies higher than that of Ag s-orbital. Therefore, Bi p-orbital mainly contributes to the anti-bonding states which show the giant RSS. If Bi p-orbital has lower energy than the atomic orbital of substrate, Bi p-orbital would mostly contribute to the bonding states, and the bonding states will show giant RSS. In that case, $|\mathrm{Bi}(p), \mathrm{downward}\rangle$ will comprise the lower band, and spin/OAM chiralities will be opposite to those of Bi/Ag(111). Controlling the direction of chirality within our scheme will further back up our asymmetric interatomic-hopping induced RSS model.

An important aspect of our model is that it tells us three conditions to have a giant RSS. First, surface states should be localized within the length scale of the atomic distance to generate significantly asymmetric charge distribution upon ISB. Then, the surface atom must have a strong atomic SOC in order to have significant OAM (J state) and thus develop $|\mathrm{upward}\rangle$ and $|\mathrm{downward}\rangle$ states under ISB. Finally, overlap between surface and subsurface orbitals should be optimized to maximize the energy difference between t_{up} and t_{dn}.

The asymmetric interatomic-hopping mechanism works in various materials with giant RSS. Considering these conditions, we argue that the asymmetric interatomic-hopping can be the dominant term for the RSS in BiTeI[20] for which Bi layer is sandwiched between Te and I layers with appropriate interatomic-hopping environment within our model. Another important example may be the surface states of Bi_2Se_3 which have one of the largest spin splitting near the Γ-point among topological insulators.[46] The asymmetric interatomic-hopping should be responsible for the large spin splitting in Bi_2Se_3 near the Γ-point, since the Bi layer is sandwiched between two inequivalent Se layers.[46]

Acknowledgments We thank David Vanderbilt for fruitful discussion. This work was supported by the Incheon National University Research Grant in 2014.

*AbePark@inu.ac.kr
†jhshim@postech.ac.kr

1) A. Manchon, H. C. Koo, J. Nitta, S. M. Frolov, and R. A. Duine, Nat. Mater. **14**, 871 (2015).
2) J. R. Bindel, M. Pezzotta, J. Ulrich, M. Liebmann, E. Ya. Sherman, and M. Morgenstern, Nat. Phys. **12**, 920 (2016).
3) Z. Qin, G. Qin, B. Shao, and X. Zuo, Nanoscale **9**, 11657 (2017).
4) H. C. Koo, J. H. Kwon, J. Eom, J. Chang, S. H. Han, and M. Johnson, Science **325**, 1515 (2009).
5) P. Chuang, S.-C. Ho, L. W. Smith, F. Sfigakis, M. Pepper, C.-H. Chen, J.-C. Fan, J. P. Griffiths, I. Farrer, H. E. Beere, G. A. C. Jones, D. A. Ritchie, and T.-M. Chen, Nat. Nanotechnol. **10**, 35 (2015).
6) A. Manchon and S. Zhang, Phys. Rev. B **78**, 212405 (2008).
7) I. M. Miron, G. Gaudin, S. Auffret, B. Rodmacq, A. Schuhl, S. Pizzini, J. Vogel, and P. Gambardella, Nat. Mater. **9**, 230 (2010).
8) J. C. Rojas Sánchez, L. Vila, G. Desfonds, S. Gambarelli, J. P. Attané, J. M. De Teresa, C. Magén, and A. Fert, Nat. Commun. **4**, 2944 (2013).
9) E. Lesne, Y. Fu, S. Oyarzun, J. C. Rojas-Sánchez, D. C. Vaz, H. Naganuma, G. Sicoli, J.-P. Attané, M. Jamet, E. Jacquet, J.-M. George, A. Barthélémy, H. Jaffrès, A. Fert, M. Bibes, and L. Vila, Nat. Mater. **15**, 1261 (2016).
10) S. Oyarzún, A. K. Nandy, F. Rortais, J.-C. Rojas-Sánchez, M.-T. Dau, P. Noël, P. Laczkowski, S. Pouget, H. Okuno, L. Vila, C. Vergnaud, C. Beigné, A. Marty, J.-P. Attané, S. Gambarelli, J.-M. George, H. Jaffrès, S. Blügel, and M. Jamet, Nat. Commun. **7**, 13857 (2016).
11) D. Di Sante, P. Barone, R. Bertacco, and S. Picozzi, Adv. Mater. **25**, 509 (2013).
12) M. Kepenekian, ACS Nano **9**, 11557 (2015).
13) V. V. Volobuev, Adv. Mater. **29**, 1604185 (2017).
14) C. R. Ast, Phys. Rev. Lett. **98**, 186807 (2007).
15) G. Bihlmayer, S. Blügel, and E. V. Chulkov, Phys. Rev. B **75**, 195414 (2007).
16) C. R. Ast, Phys. Rev. B **77**, 081407 (2008).
17) F. Meier, H. Dil, J. Lobo-Checa, L. Patthey, and J. Osterwalder, Phys. Rev. B **77**, 165431 (2008).
18) G. Bian, L. Zhang, Y. Liu, T. Miller, and T.-C. Chiang, Phys. Rev. Lett. **108**, 186403 (2012).
19) L. El-Kareh, P. Sessi, T. Bathon, and M. Bode, Phys. Rev. Lett. **110**, 176803 (2013).
20) K. Ishizaka, Nat. Mater. **10**, 521 (2011).
21) A. Crepaldi, Phys. Rev. Lett. **109**, 096803 (2012).
22) G. Landolt, Phys. Rev. Lett. **109**, 116403 (2012).
23) X. Xi, Phys. Rev. Lett. **111**, 155701 (2013).
24) Y. A. Bychkov and É. I. Rashba, JETP Lett. **39**, 78 (1984).
25) S. LaShell, B. A. McDougall, and E. Jensen, Phys. Rev. Lett. **77**, 3419 (1996).
26) L. Petersen and P. Hedegård, Surf. Sci. **459**, 49 (2000).
27) S. R. Park, C. H. Kim, J. Yu, J. H. Han, and C. Kim, Phys. Rev. Lett. **107**, 156803 (2011).
28) B. Y. Kim, P. J. Kim, W. Jung, Y. K. Kim, Y. Y. Koh, W. S. Kyung, J. B. Park, M. Matsunami, S. Kimura, J. S. Kim, J. H. Han, and C. Kim, Phys. Rev. B **88**, 205408 (2013).
29) J. Hong, J.-W. Rhim, C. Kim, S. R. Park, and J. H. Shim, Sci. Rep. **5**, 13488 (2015).
30) V. Sunko, H. Rosner, P. Kushwaha, S. Khim, F. Mazzola, L. Bawden, O. J. Clark, J. M. Riley, D. Kasinathan, M. W. Haverkort, T. K. Kim, M. Hoesch, J. Fujii, I. Vobornik, A. P. Mackenzie, and P. D. C. King, Nature **549**, 492 (2017).
31) M. Hirayama, R. Okugawa, T. Miyake, and S. Murakami, Nat. Commun. **8**, 14022 (2017).
32) G. Kresse and J. Hafner, Phys. Rev. B **47**, 558 (1993).
33) G. Kresse and J. Hafner, Phys. Rev. B **49**, 14251 (1994).
34) G. Kresse and J. Furthmüller, Comput. Mater. Sci. **6**, 15 (1996).
35) G. Kresse and J. Furthmüller, Phys. Rev. B **54**, 11169 (1996).
36) T. Ozaki, Phys. Rev. B **67**, 155108 (2003).
37) T. Ozaki and H. Kino, Phys. Rev. B **69**, 195113 (2004).
38) T. Ozaki and H. Kino, Phys. Rev. B **72**, 045121 (2005).
39) J. P. Perdew, K. Burke, and M. Ernzerhof, Phys. Rev. Lett. **77**, 3865 (1996).
40) J. C. Slater and G. F. Koster, Phys. Rev. **94**, 1498 (1954).
41) (Supplemental Material) DFT analysis depending on Δz and details on tight binding analysis are provided online.
42) K. Momma and F. Izumi, J. Appl. Crystallogr. **44**, 1272 (2011).
43) G. Bian, X. Wang, T. Miller, and T.-C. Chiang, Phys. Rev. B **88**, 085427 (2013).
44) S. Schirone, E. E. Krasovskii, G. Bihlmayer, R. Piquerel, P. Gambardella, and A. Mugarza, Phys. Rev. Lett. **114**, 166801 (2015).
45) I. Gierz, B. Stadtmüller, J. Vuorinen, M. Lindroos, F. Meier, J. H. Dil, K. Kern, and C. R. Ast, Phys. Rev. B **81**, 245430 (2010).
46) H. Zhang, C.-X. Liu, X.-L. Qi, X. Dai, Z. Fang, and S.-C. Zhang, Nat. Phys. **5**, 438 (2009).